AIAA 79-1629R

Factors Affecting the Fluctuating Pressures on Ablated and Unablated Re-entry Nosetips

J. Peter Reding,* Y. John Kaku,† and Rolf A. Guenther†
Lockheed Missiles & Space Co., Inc., Sunnyvale, Calif.

Fluctuating pressure measurements have been obtained at $M=5.0$ on hemispherical, blunt-conic, and indented nosetips that simulate the evolution of an ablating graphite nosetip during re-entry. An analysis of the fluctuating pressure distribution data on hemispherical and blunt-conic nosetips shows that when the flow is attached, as it is for these noses, the fluctuating pressure spectra can be collapsed successfully using freestream flow parameters rather than boundary-layer parameters. The spectra from the indented nosetip are collapsed with freestream flow parameters and the maximum thickness of the region of flow separation. It is postulated that entropy gradient effects, not the boundary shear, dominant the fluctuating pressures when the flow is attached, and that flow separation effects dominate the fluctuating pressures when the flow is separated.

Nomenclature

a = speed of sound, m/s
C_p = pressure coefficient $(p-p_\infty)/q$
$C_{p(\text{rms})}$ = root-mean-square fluctuating pressure coefficient, p_{rms}/q
f = frequency, Hz
M = Mach number, U/a
M_e = local Mach number at boundary-layer edge
PSD = power spectral density, $(\text{kg/m}^2)^2/\text{Hz}$
p = local pressure, kg/m^2
p_∞ = freestream static pressure, kg/m^2
$p(t)$ = time varying pressure, kg/m^2
p_{rms} = fluctuating pressure $\frac{1}{\tau}\int_0^\tau \left[(p(t)-p)^2\right]^{1/2} dt$, kg/m^2
q = freestream dynamic pressure, $\rho U^2/2$, kg/m^2
q_e = local dynamic pressure at boundary-layer edge, kg/m^2
R = freestream Reynolds number, m^{-1}
R_e = Reynolds number at boundary-layer edge
R_N = Reynolds number based on nose radius
r_N = nose radius, m
T = temperature, °C
t = time, s
$\Delta T/\Delta t$ = temperature rise rate, °C/s
U = freestream velocity, m/s
U_e = local velocity at boundary-layer edge, m/s
x = axial coordinate, m
α = angle of attack, deg
Δ = increment
δ = boundary-layer thickness, m
δ_m = maximum separated flow height, m
ρ = freestream density, $\text{kg-s}^2/\text{m}^4$
θ = angular position of transducer relative to model centerline, deg
ϕ = roll orientation of transducer relative to top ($\phi=0$) meridian, deg

Presented as Paper 79-1629 at the AIAA Atmospheric Flight Mechanics Conference, Boulder, Colo., Aug. 6-8, 1979; submitted Oct. 23, 1979; revision received April 14, 1980.

*Staff Engineer. Associate Fellow AIAA.
†Research Specialist.

Introduction

DURING re-entry, an initially spherical nosetip experiences significant shape changes due to the effects of ablation. First, the spherical nose flattens due to laminar ablation in the stagnation region. This is followed by a blunt-cone shape as transition moves onto the sides of the nosetip increasing ablation locally. As transition persists on the sides, the nosetip begins to cusp and eventually resembles a spiked cone or a "tension shell" body. Finally, the spike tip ablates away entirely, and the nosetip becomes roughly conic. The ablation-induced shape change alters the re-entry body drag and stability. Trim can also occur as a result of shape asymmetries caused by asymmetries in the transition front or material inhomogeneities or both.

Nosetip shape changes also affect the fluctuating pressures on the nosetip which, in turn, can impact nosetip structural integrity. It has long been recognized that periodic pressure oscillations can occur on the highly indented noses. These periodic pressure oscillations are the result of a gross instability of the separated flow region that dominates the severely indented nosetips.[1-4] Large random pressure fluctuations are associated with the so-called steady separated flow[4] of noncritical geometries. Recently fluctuating pressure measurements have been obtained on mildly indented and blunt-conic nosetips[5] that are typical of sections of an ablated graphite nosetip of the nosetip recovery vehicle (NRV)[6] and of wind tunnel ablated camphor nosetips.[7] Even replicas of the NRV and low temperature ablated noses were tested. However, the instrumentation density was insufficient to define the fluctuating pressure distribution. Subsequently, further wind tunnel tests were conducted to obtain detailed fluctuating pressure distribution data on three idealized, axisymmetric models that simulate the three fundamental stages in the evolution of an ablating graphite nosetip: hemispherical, blunt conic, and indented. An analysis of these data is presented herein.

Wind Tunnel Test

To supply the fluctuating pressure distribution data needed to determine nosetip structural integrity and to establish scaling criteria between wind tunnel and flight, a wind tunnel test was conducted in the Naval Surface Weapons Center, White Oak Laboratory, Tunnel 8[8] at $M=5.0$ and $1.6\times10^7/\text{m} \le R \le 13.1\times10^7/\text{m}$. Three axisymmetric nosetip models were tested: hemispherical, blunt conic, and indented. These models were instrumented with either four of five Kulite fluctuating pressure transducers (located as shown in Fig. 1) that had a 70,000-Hz resonant frequency. Data were

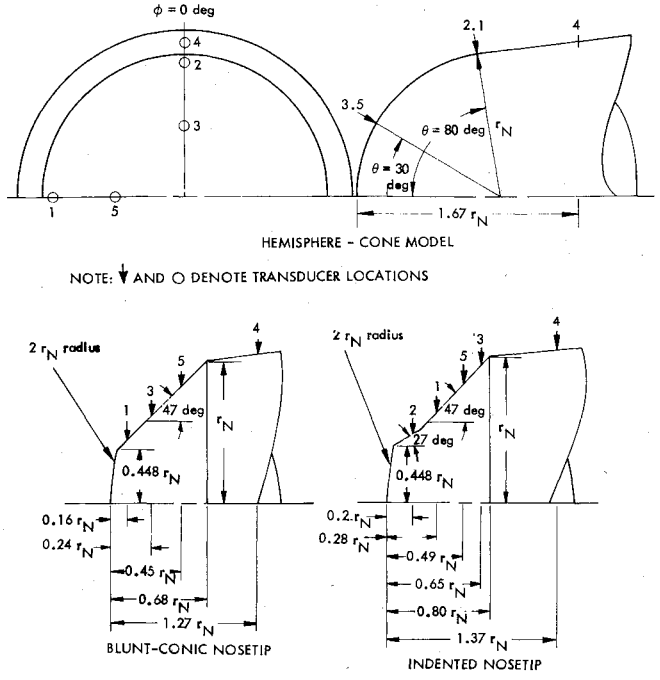

Fig. 1 Wind tunnel model configurations.

recorded over the frequency range of 200-45,000 Hz and reduced in 250-Hz bandwidths.

These were the same models used in previous static and fluctuating[5] pressure tests with the exception of the hemispherical nosetip. A new thin-walled hemispherical nose was especially constructed to allow simultaneous heat transfer and fluctuating measurements so that the location of transition could be correlated with the fluctuating pressure distributions.

As is usual with wind tunnel fluctuating pressure measurements, the effects of background noise were a major concern. Thus, every effort was made to minimize electrical system noise and to ensure that the fluctuating pressure measurements were sufficiently above wind tunnel background noise levels. Measurements were taken of the model in a quiet test cabin, and the recorded signal—indicative of total system (microphone-amplifier-recorder) electrical noise—was reduced to an overall fluctuating pressure coefficient. These values are compared to wind tunnel background noise data in Fig. 2.[9] The worst electrical noise is two to three orders-of-magnitude below the wind tunnel background noise. Thus, the effort to minimize electrical noise was eminently successful, and it is the wind tunnel background noise that must be considered.

Figure 2 indicates that wind tunnel background noise will limit the validity of the data. The data were judged valid if the power spectra were at least an order of magnitude above background noise levels throughout the frequency range, as illustrated by the comparison of the background noise spectrum from Ref. 9 with the marginally valid data measured at $\theta = 80$ deg on the hemispherical nosetip at a nearly identical Reynolds number (Fig. 3).

Unfortunately, power spectral measurements of the background noise are not available for all Reynolds numbers. Only the overall fluctuating pressure coefficient $C_{p(\text{rms})}$, values are available vs Reynolds number. Because $C_{p(\text{rms})}$ is the square root of the integral of the power spectra, an equivalent criterion is

$$C_{p(\text{rms})D} \geq \sqrt{10}\, C_{p(\text{rms})N} \qquad (1)$$

where D denotes data and N background noise. This tacitly assumes similar shaped spectra for both the data and the

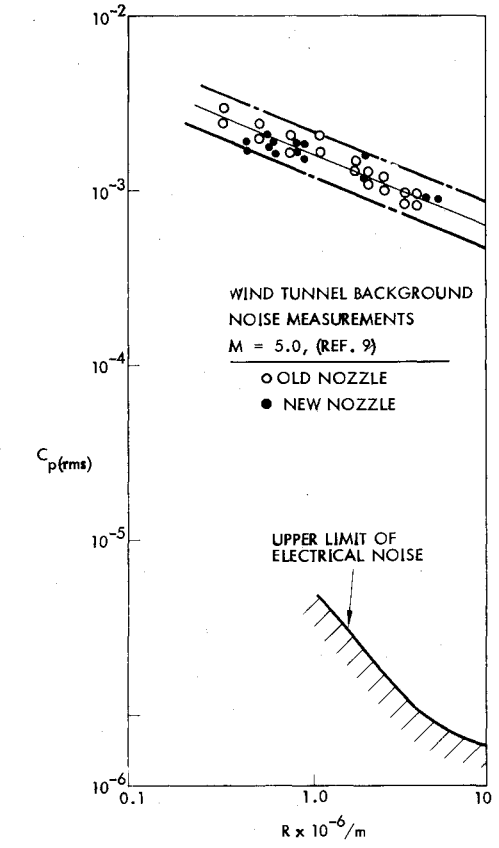

Fig. 2 Comparison of wind tunnel background noise and electrical noise.

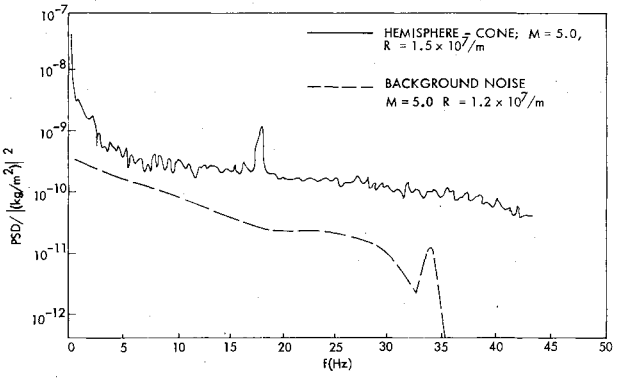

Fig. 3 Comparison of a typical boundary-layer spectrum with background noise.

background noise. Spikes in the background noise spectra and a radically different spectral shape will invalidate the criterion unless $C_{p(\text{rms})D}$ values are well (orders of magnitude) above the $C_{p(\text{rms})N}$ values. The one background noise spectrum available[9] tends to substantiate the similar spectra assumption (Fig. 3).

Note that the roll off of the background noise at 35,000 Hz (Fig. 3) is the result of a low-pass filter and does not indicate actual background noise characteristics. However, the effect of the filter on $C_{p(\text{rms})N}$ is negligible causing less than a 0.01% reduction.

Only data that meet the validity criterion of Eq. (1) are presented herein (e.g., Fig. 4). In many cases, the data exceed background noise values by more than an order of magnitude. In these cases, the assumption of similar spectra is not nearly so critical. There is a consistency in the spectra for these very high $C_{p(\text{rms})}$ values, which almost certainly are valid, and the spectra for $C_{p(\text{rms})}$ values that just meet the validity criterion.

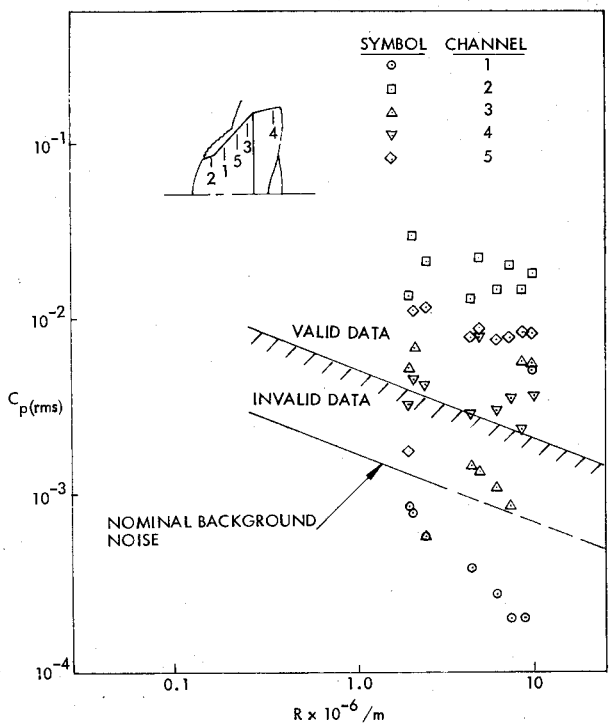

Fig. 4 Validity of indented nose data.

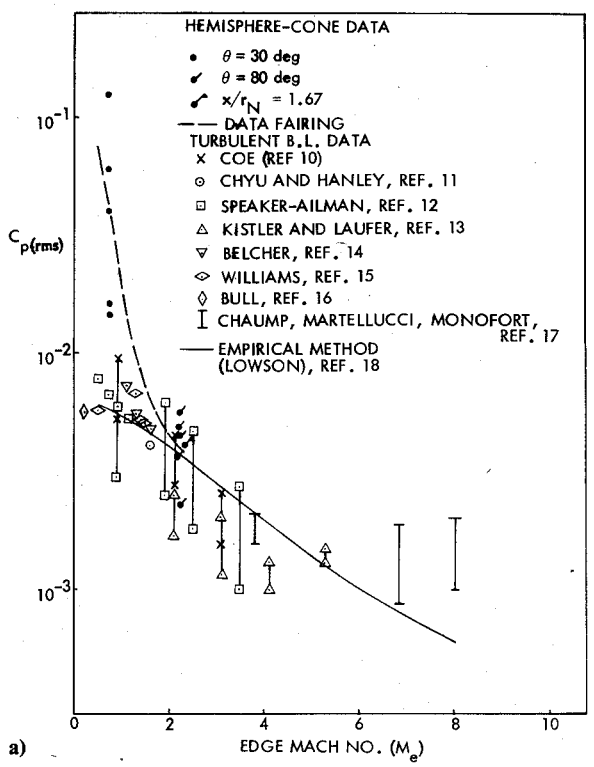

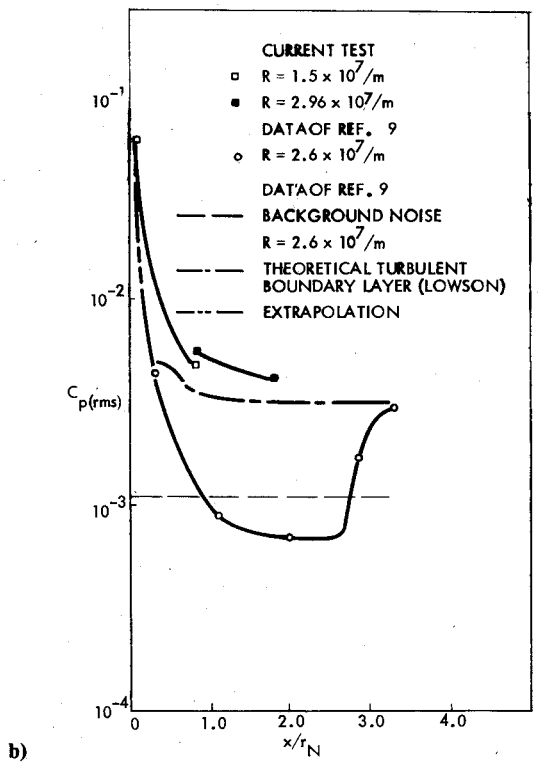

Fig. 5 Comparison of overall fluctuating pressure data for the hemisphere cone: a) with turbulent boundary-layer data, and b) fluctuating pressure distributions.

This tends to substantiate the validity of the lower measurements. Such consistency will become evident in the comparison of normalized spectra presented later in the paper.

Data Analysis

The goal of the data analysis is to find a means of normalizing the wind tunnel data. This will provide a method of scaling wind tunnel data to flight conditions and also will provide insight into the flow phenomena responsible for the pressure fluctuations.

Hemispherical Nosetip

Valid rms fluctuating pressure coefficient data obtained from the present hemispherical nosetip are compared with both two- and three-dimensional turbulent boundary-layer measurements[10-17] and with Lowson's[18] semiempirical prediction technique (Fig. 5a). The agreement is good except for the most forward measurements taken only 30 deg from the stagnation point (at $\theta = 30$ deg). Earlier results obtained in the same wind tunnel by Baltakis (Fig. 5b) also indicate the possibility of elevated fluctuating pressure levels near the stagnation point.[19]

Transition occurs further upstream in the present test than it did in Baltakis' test (Fig. 5b).[19] Baltakis' data indicate transition occurred nearly three nose radii downstream of the stagnation point at $R = 2.6 \times 10^7$/m, whereas the present data indicate transition occurred on the spherical portion of the nose near $\theta = 30$ deg ($x/r_N = 0.13$) for nearly the entire Reynolds number range tested (Fig. 6). Schlieren photographs obtained in another test[20] in the same wind tunnel at $R = 16.6 \times 10^7$/m indicate transition also occurred on the sphere between $\theta = 50$ and 70 deg which is in better agreement with the present results.

The earlier transition in the present test may be the result of severe pitting of the nosetip because of impacts by tunnel contaminants. Particles of the zirconia pellets that make up the thermal mass of the tunnel (which prevents liquefaction of the air) evidently were carried into the tunnel and impacted the model causing pitting of the nosetip. (Incidentally, this problem has now been cured with the installation of a particle catcher in the stilling chamber). The particle impact destroyed the microphones at $\theta = 30$ deg early in the test. Thus, only low Reynolds number data are available at $\theta = 30$ deg.

Baltakis' data show that the state of the boundary layer (laminar or turbulent) has an effect on the overall fluctuating pressure level with the higher fluctuating pressure occurring under the turbulent boundary layer.[19] Also, both tests show the fluctuating pressure increases above turbulent values near

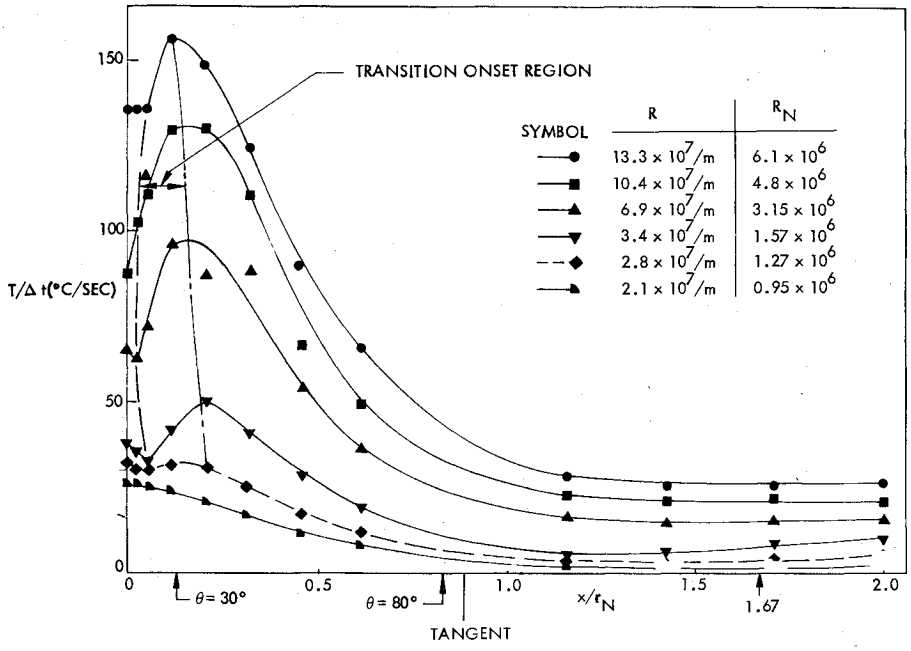

Fig. 6 Transition locations on the hemisphere cone.

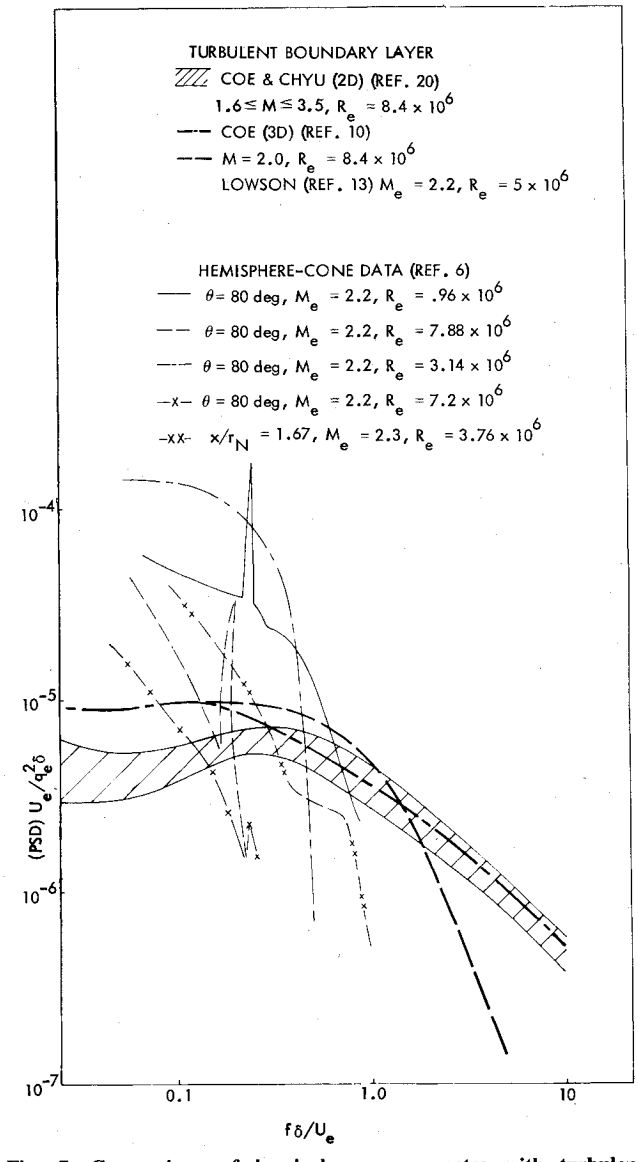

Fig. 7 Comparison of hemisphere-cone spectra with turbulent boundary-layer spectra.

the stagnation point even if the boundary layer is laminar (Fig. 5b).

Power-spectral-density measurements under the turbulent portion of the boundary layer have been nondimensionalized with boundary-layer edge properties. These nondimensional spectra do not agree with either the two-dimensional data of Coe and Chyu,[21] the three-dimensional data of Coe,[10] or the semiempirical method of Lowson.[18] Not only do the present data show a large scatter, but the shape of the nondimensional spectra is quite different from the other experimental results and the semiempirical theory.

Note that the boundary-layer thickness and edge properties used to nondimensionalize the spectra in Fig. 7 were not measured in the wind tunnel; rather the velocity, edge dynamic pressure, and boundary thickness were computed using correlated method of characteristics results and integral boundary-layer methods as mechanized in the GRANT 3D computer code.[22] Thus, there are undoubtedly some differences between these estimates and the actual boundary-layer thickness and edge conditions. However, such differences certainly could not have been large enough to account for the nearly two order of magnitude spread in the nondimensional spectra shown in Fig. 7.

The spectra from under both the transitional and turbulent portions of the boundary layer on the hemisphere cone have been further normalized with the local conditions by dividing by $[C_{p(\mathrm{rms})}]^2$ (Fig. 8). The turbulent boundary-layer spectra ($\theta = 80$ deg and $x/r_N = 1.67$) and the transitional spectra at $\theta = 30$ deg do not overlay one another but string out end to end.

It is well known that at hypersonic speeds, the curved bow shock caused by the hemispherical nosetip dominates the static pressure distribution for many nose radii downstream of the tip.[23] The highly nonlinear fluctuating pressure distribution for the hemisphere cone in Fig. 5 suggests that entropy wake effects may also dominate the fluctuating pressures over the nosetip.

If the pressure fluctuations on the nosetip are truly dominated by the nonuniform flow effects of the curved bow shock, then freestream flow parameters and a length characteristic of the bow shock curvature would seem more logical scaling parameters. Thus, the spectra from the hemisphere cone have been nondimensionalized with the nose radius (r_N), freestream flow conditions, and $[C_{p(\mathrm{rms})}]^2$ (Fig. 9). The collapse of the spectra using freestream properties is

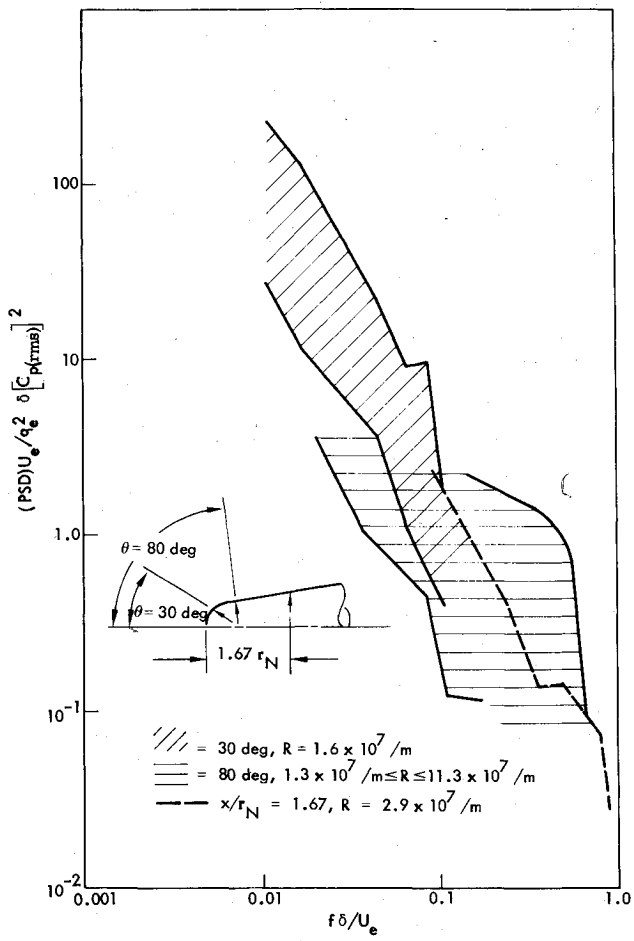

Fig. 8 Spectra for the hemisphere cone normalized with boundary-layer edge properties.

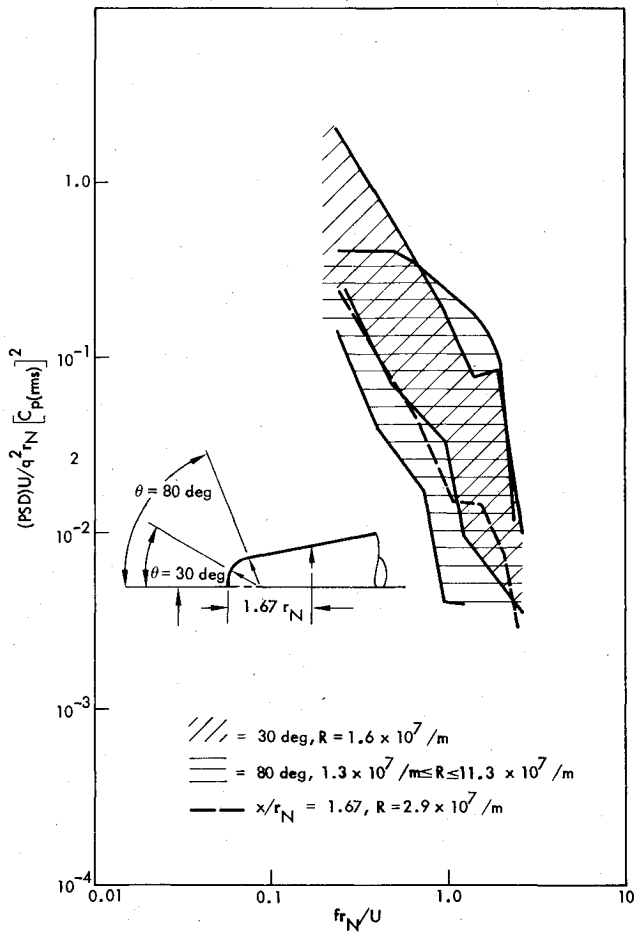

Fig. 9 Spectra for the hemisphere cone normalized with freestream flow properties.

superior to that obtained using edge properties (compare Figs. 8 and 9). The spectra nondimensionalized with edge properties tend to string out end to end where the spectra nondimensionalized with freestream flow parameters overlay one another. The data spread also is reduced using freestream parameters; however, the improvement is not dramatic. The superior collapse of the data along the nosetip tends to substantiate the validity of the freestream properties as scaling parameters. It is believed that spread of the normalized spectra is wide (Fig. 9) because the data just barely meet the validity criterion, and may not be entirely free of background noise effects.

Blunt-Conic Nosetip

The data from the blunt-conic nosetip are clearly far from marginal. They solidly exceeded the validity criterion (by over an order of magnitude in some instances) except for the data from transducer number 4 which is entirely invalid. The good agreement with measurements from Ref. 5 tends to further substantiate confidence in the validity of the current data (Fig. 10).

Data from transducers 3 and 5 where the boundary layer is turbulent[20]‡ have been normalized using the local boundary-layer thickness and edge conditions from the GRANT 3D code. As before, the computed edge properties cannot be so much in error as to cause the nearly two order of magnitude difference in the nondimensional spectra shown in Fig. 11.

The spectral data for the blunt-conic model have been nondimensionalized using both boundary-layer edge conditions and freestream conditions (Figs. 12 and 13). The

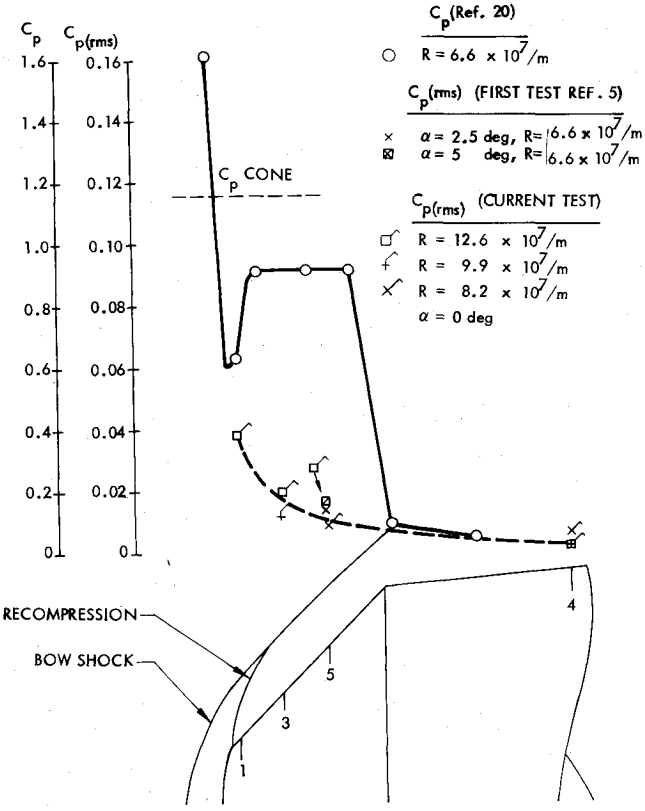

Fig. 10 Comparison of static and fluctuating pressures for the blunt-conic nosetip.

‡Schlieren photographs from Ref. 20 indicate transition occurred in the vicinity of transducer 1 at $R = 6.64\ 10^7$/m.

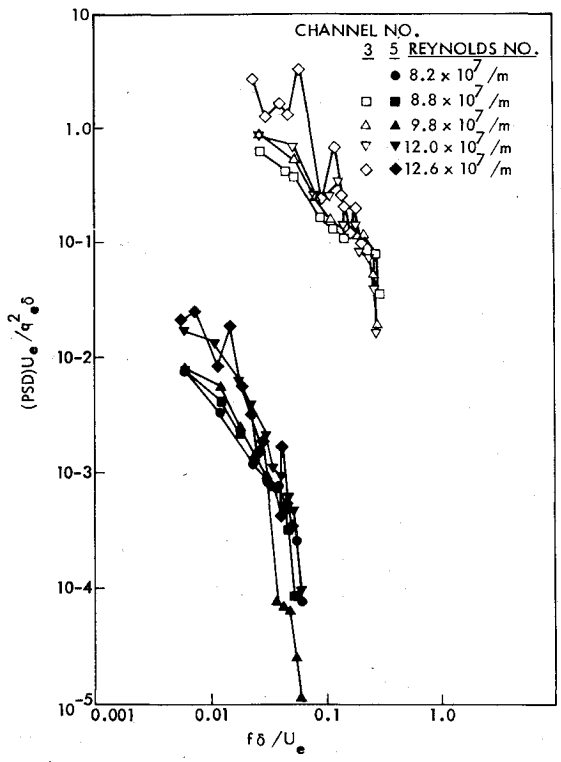

Fig. 11 Comparison of turbulent spectra for the blunt-conic model normalized with boundary-layer edge properties.

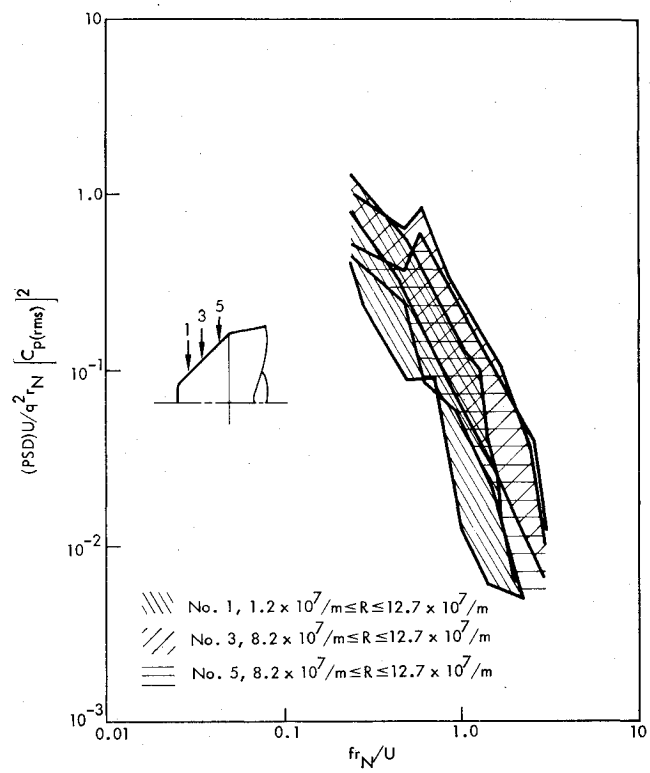

Fig. 13 Spectra for the blunt-conic nosetip normalized with freestream flow properties.

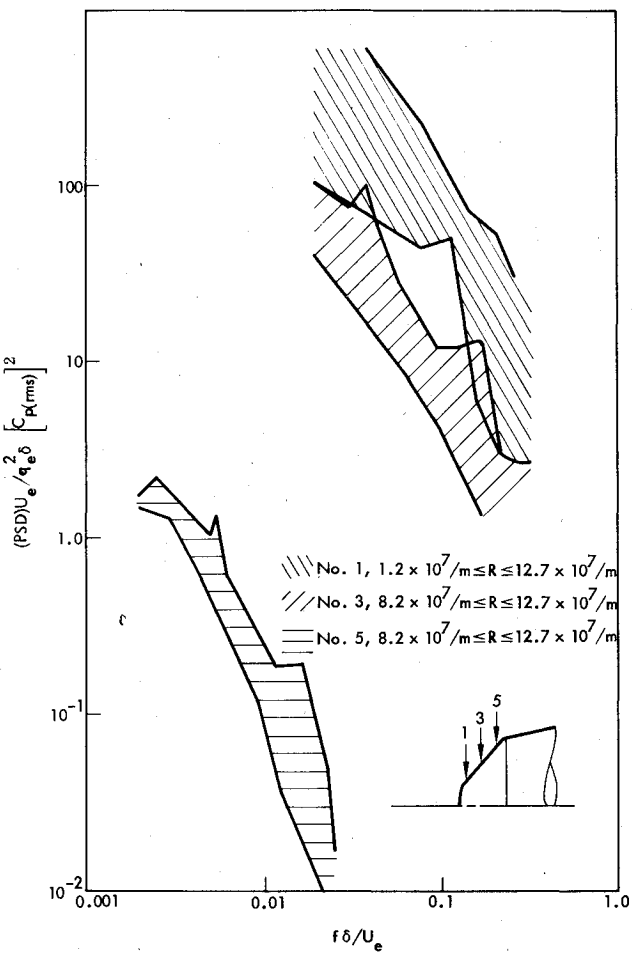

Fig. 12 Spectra for the blunt-conic nosetip normalized with boundary-layer edge properties.

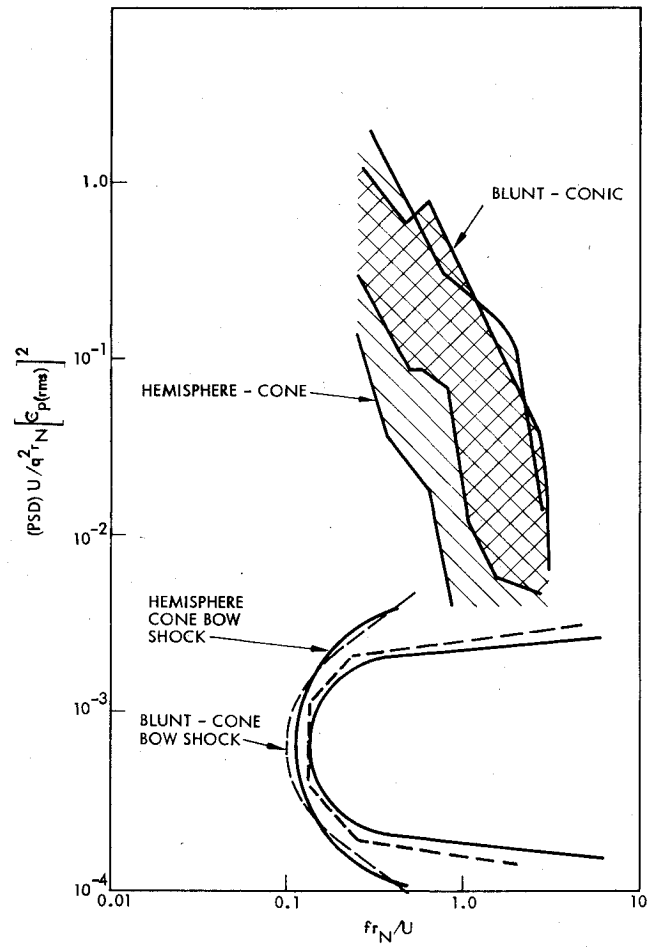

Fig. 14 Comparison of normalized spectra on hemisphere cone and blunt-conic nosetip.

collapse using freestream flow conditions is obviously superior. This suggests that entropy gradient effects dominate the fluctuating pressures on the blunt-conic nosetip.

Generally, the shape of the spectra from the blunt-conic and the hemispherical nosetips are similar, although the data spread for the blunt-conic nosetip is much tighter (Fig. 14). This is undoubtedly the result of their similar shock shapes (inset in Fig. 14), thus, their similar entropy gradients.

Unfortunately, because of transducer temperature limitations, it was impossible to obtain data at higher Mach numbers. Thus, the scaling techniques used to collapse the spectra of this, and the hemispherical nosetip, are valid only at one Mach number. It is postulated that Mach number effects could be accounted for by using a length scale indicative of the radius of curvature of the bow shock which will, of course, vary with Mach number. Another technique might be to define how $C_{p(\text{rms})}$ varies with Mach number, and use this variation to account for Mach number effects. Perhaps a combination of both approaches could prove successful. Regardless, it is evident that how Mach number affects the pressure fluctuations on re-entry nosetips is unknown and can be answered only by further experimental and theoretical research.

Indented Nosetip

A substantial amount of the data for the indented nosetip are well above the validity criterion (Fig. 4). Unfortunately most of the data from transducers 1 and 3 are invalid. A comparison of the overall fluctuating pressure distributions with the data from Ref. 5 shows mixed results (Fig. 15). The agreement under the separated region is good whereas the agreement in the reattachment region is not so good. Angle-of-attack differences between the two tests are believed to be the cause of the poor agreement. As it turned out, the model was mounted so that the instrumented ray was down in the present test whereas it was up in an earlier test.[5] When one considers the combined effects of flow angularity in the wind tunnel and the tolerances involved in achieving a given angle of attack, the angle-of-attack difference between the two tests could easily have been $\alpha = \pm 0.5$ deg. Thus, transducer 5 easily could have missed the very sharp fluctuating pressure peak at reattachment. However, spectral data show that it still was located within the reattachment region.

Data from the previous tests of the indented nosetip[5] showed an indication of transition in the lifted shear layer over the separated region for $R = 3.3 \times 10^7$/m. However, this disappeared for $R \geq 6.6 \times 10^7$/m, indicating turbulent separation exists in this Reynolds number range. Thus, the data presented herein for $R \geq 6.6 \times 10^7$/m are taken to be indicative of turbulent separation.

Earlier results have established that separated flow effects dominate the fluctuating pressure environment of indented nosetips.[5] Furthermore, the technique of nondimensionalizing the spectra with freestream flow parameters and the maximum height of the separated region successfully collapsed the spectra in the reattachment region of a variety of spike-induced separated flows.[5,23] The data from the present test are no exception (Fig. 16).

The maximum separated flow height δ_m is measured in a direction normal to the body axis from the surface to the top of the separated region as indicated by shadowgraph photographs (see inset in Fig. 16).

Essentially two types of spectra occur in the indented portion of the nosetip (Fig. 16). One is associated with flow reattachment, the other with the environment under the flow separation. The difference between the reattachment and separated flow spectra reflect the influence of the portion of the boundary layer, the lifted shear layer, that passes over the separated region through reattachment and continues downstream.

The shear layer does not enter the recirculation region, and therefore does not affect the environment under the separated region. This explains the difference between the separated flow and the reattachment spectra for $0.01 \leq f\delta_m/U \leq 0.2$ (Figs. 17a and b). The shear layer does, however, influence the spectra both at reattachment and downstream of reattachment as indicated by the similarly shaped spectra (compare Figs. 17b and c). The good agreement between the present data and the data of Ref. 5 substantiates the validity of the present measurements.

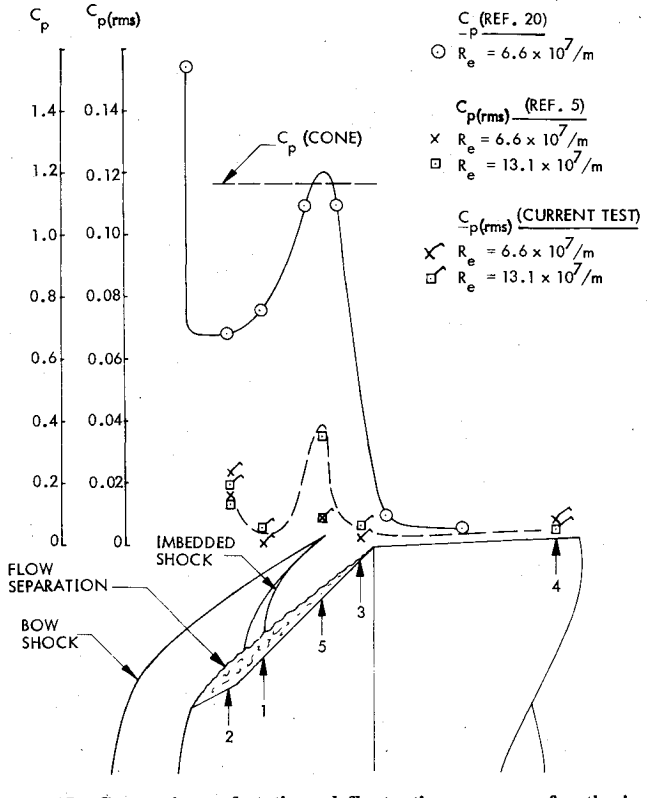

Fig. 15 Comparison of static and fluctuating pressures for the indented nosetip.

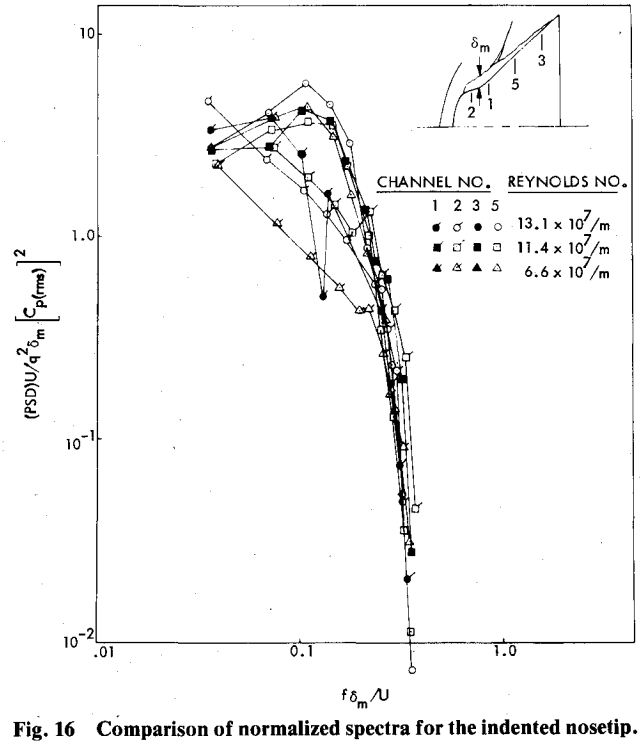

Fig. 16 Comparison of normalized spectra for the indented nosetip.

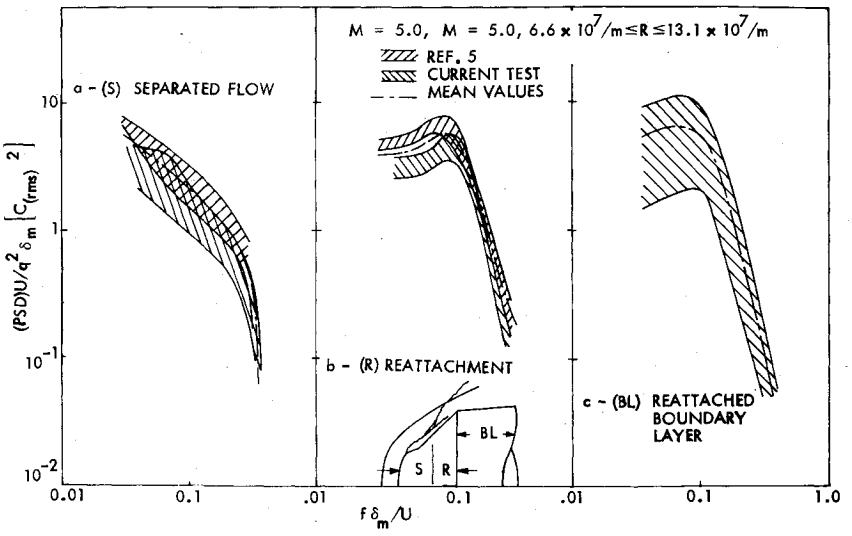

Fig. 17 Normalized spectra from various regions of the indented nosetip.

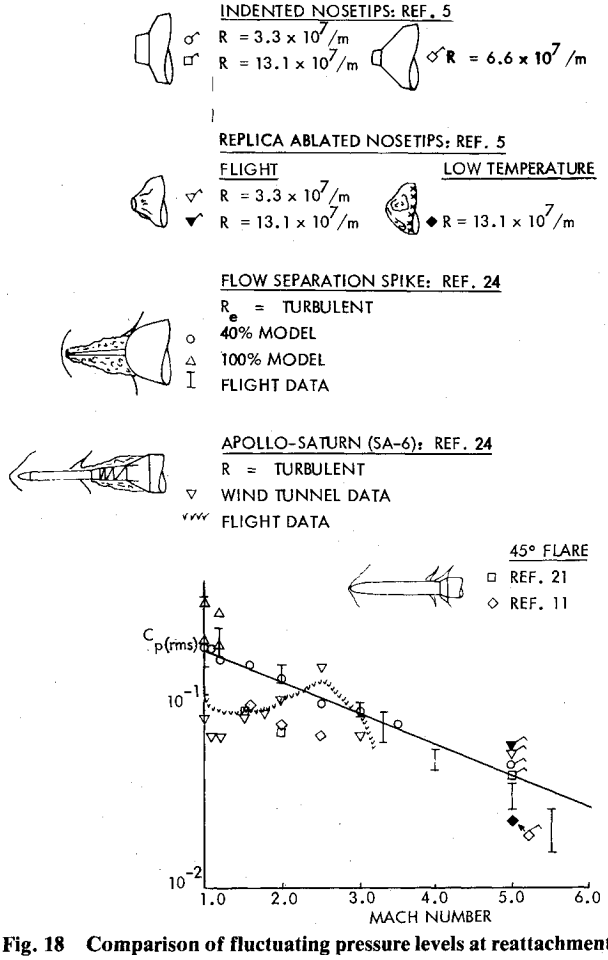

Fig. 18 Comparison of fluctuating pressure levels at reattachment.

Unfortunately, these results are valid for only a single Mach number. However, previous results show how the overall fluctuating pressure coefficient, $C_{p(\mathrm{rms})}$ in the reattachment region of spike-induced flow separations varies with Mach number (Fig. 18).[5] This may be the key to the Mach number scaling. One would expect that a similar variation should occur throughout the separated region. Thus, by accounting for the variation of $C_{p(\mathrm{rms})}$ with Mach number, one might be able to collapse the separated flow spectra for all Mach numbers. Of course, more data must be secured and analyzed before the question of Mach number scaling can be answered.

Conclusions

An analysis of wind tunnel measurements, taken at $M=5.0$, of the fluctuating pressure environment on models simulating ablated and unablated re-entry nosetips has shown that as long as the boundary layer is attached, regardless whether the nosetip geometry has been altered by ablation or not, entropy gradient effects dominate the fluctuating pressure spectra although boundary-layer transition affects the overall fluctuating pressure level. Thus, the fluctuating pressure spectra scale with freestream flow properties and the spherical nose radius. When the nose is indented enough to cause flow separation, the flow separation effects dominate the pressure fluctuations and the spectra scale with freestream flow conditions and the maximum height of the separated flow region.

Unfortunately, these results are valid only for a single, constant Mach number. Thus, the effects of Mach number on the fluctuating pressure environment are unknown. It has been suggested that when the flow is attached, a Mach number dependent length scale proportional to the bow shock radius of curvature, a Mach number dependent variation of $C_{p(\mathrm{rms})}$, or some combination of both might be used to account for Mach number effects. The overall fluctuating pressure $C_{p(\mathrm{rms})}$ in the reattachment region of spike induced flow separation has already been observed to vary with Mach number. It has been suggested that further investigation of this phenomenon could lead to a technique for Mach number scaling of the fluctuating pressure spectra on indented noses.

Of course, ablation will also affect the pressure fluctuations on re-entry nosetips in flight. One would expect that ablation effects would be most significant where viscous effects dominate the pressure fluctuations as they do for the indented nosetips. Where entropy gradient effects dominate, ablation effects should be less important.

All this only serves to illustrate that we are just beginning to understand the fluctuating pressure environment on re-entry nosetips. Much experimental and theoretical work remains to be done. Probably, the next step is an experimental investigation of the effects of Mach number on nosetip fluctuating pressures.

Acknowledgment

The authors express appreciation to R.T. Driftmyer, Naval Surface Weapons Center, who conducted the wind tunnel tests and supervised the data reduction.

References

[1] Baltakis, F.P., "Wind Tunnel Study of Oscillating Flow-Induced Surface Pressures on a Tension-Cone Geometry Model," Naval Ordnance Laboratory Tech. Rept. NOL TR 74-134, Jan. 1974.

[2] Wood, C.J., "Hypersonic Flow over Spiked Cones," *Journal of Fluid Mechanics,* Vol. 12, Pt. 4, April 1962.

[3] Kabelitz, H.P., "Zur Stabilität geschlossener Grenzschichtablösegebiete an Konischen Drehkörpen bei Hyperschallanströmung," DLB FB 71-77, July 1971.

[4] Abbett, M.J., Cooper, L., Dahm, T.J., and Jackson, M.D., "Unsteady Flow on Ablated Nosetip Shapes, Pant Series G, Test and Analysis Report," Aerotherm Rept. 73-87, Dec. 1973.

[5] Reding, J.P., "Fluctuating Pressures on Mildly Indented Nosetips," *Journal of Spacecraft and Rockets,* Vol. 16, Sept.-Oct. 1979, pp. 302-310.

[6] Otey, G.R. and English, E.A., "High-β Re-entry Vehicle Recovery," *Journal of Spacecraft and Rockets,* Vol. 14, May 1977, pp. 290-293.

[7] Wallace, G.A., "Wind Tunnel Test Series Conducted for LMSC, Part I Low Temperature Scallop Formation and Growth Rate," Acurex Corp., Aerotherm Div., Aero Therm Rept. 75-147, June 1975.

[8] Baltakis, F.P., "Performance Capability of the NOL Hypersonic Tunnel," U.S. Naval Ordnance Laboratory, NOL TR 68-157, Oct. 1968.

[9] Baltakis, F.P., "Wind Tunnel Study of Scallop Growth and Scallop Roughness Effects on Nosetip Turbulent Heat Transfer," U.S. Naval Ordnance Laboratory, Wind Tunnel Rept. 98, March 1975.

[10] Coe, C.F., "Surface Pressure Fluctuations Associated with Aerodynamic Noise," *Basic Aerodynamic Noise Research,* NASA SP-207, July 1969, pp. 409-424.

[11] Chyu, W.J. and Hanly, R.D., "Power and Cross-Spectra and Space-Time Correlations of Surface Fluctuating Pressures at Mach Numbers Between 1.6 and 2.5," AIAA Paper 68-67, New York, N.Y., June 1968.

[12] Speaker, W.V. and Ailman, C.M., "Spectra and Space-Time Correlations of the Fluctuating Pressures at a Wall Beneath a Supersonic Turbulent Boundary Layer Perturbed by Steps and Shock Waves," NASA CR-486, May 1969.

[13] Kistler, A.L., "Fluctuating Wall Pressure Under a Separated Supersonic Flow," *Journal of the Acoustic Society of America,* Vol. 36, March 1964, p. 543.

[14] Belcher, P.M., "Prediction of Boundary Layer Turbulent Spectra and Correlation for Supersonic Flight," Paper presented at the Fifth International Congress of Acoustics, Liege, Belgium, Sept. 1965.

[15] Williams, D.J.M., "Measurement of the Surface Pressure Fluctuations in Turbulent Boundary Layers," Univ. of Southhampton, A.A.S.U. Rept. 162, Dec. 1960.

[16] Bull, M.K., Willis, J.F., and Blackburn, D.P., "Wall Pressure Fluctuations in Boundary Layer Flow and Response of Simple Structures to Random Pressure Fields," A.A.S.U. Rept. 243, July 1963.

[17] Champ, L.E., Martellucci, A., and Monfort, A., "Aeroacoustic Loads Associated with High Beta Re-entry Vehicles," Wright-Patterson Air Force Base, Ohio, AFFDL-TR-72-138, May 1973.

[18] Lowson, M.V., "Prediction of Boundary Layer Pressure Fluctuations," Wright-Patterson Air Force Base, Ohio, AFFDL-TR-67-167, July 1967.

[19] Baltakis, F.P., "Transition Detection on a Sphere-Cone Nosetip with Fast-Response Pressure Transducers," U.S. Naval Ordnance Laboratory, Wind Tunnel Rept. 70, March 1973.

[20] Driftmyer, R.T., Regan, F.J., and Ragsdale, W.C., "Summary of the R198 LN Pressure Wind Tunnel Test Program, Mach 5 and 9," Naval Surface Weapons Center, White Oak Laboratory, Wind Tunnel Rept. 121, Jan. 1977.

[21] Coe, C.F. and Chyu, W.J., "Pressure-Fluctuation Inputs and Response of Panels Underlying Attached and Separated Turbulent Boundary Layers," NASA TM-X 62, 189, Sept. 1972.

[22] Chin, J.H., "Graphite Nosetip Thermal 3-D (GRANT-3D) Response Code Analysis and Computer Users' Manual," Lockheed Missiles and Space Co. Inc., Rept. LMSC/D366946, Nov. 1974.

[23] Sieff, A., "Secondary Flow Fields in Hypersonic Shock Layers," NASA, TN D-1304, 1962.

[24] Reding, J.P., Guenther, R.A., and Jecmen, D.M., "Scale Effects on the Fluctuating Pressures in a Region of Spike-Induced Flow Separation," AIAA Paper 79-0143, New Orleans, La., Jan. 1979.